Seasonality of amino acid enantiomers and microbial communities at MOLA time series in the NW Mediterranean Sea

Anabel von Jackowski, Quentin-Boris Barral, Nawal Bouchachi, Barbara Marie, Olivier Crispi, Paul Labatut, Karine Escoubeyrou, Charles-Hubert Paulin, Celine Dimier, Josephine Ras, et al.

Seasonality of amino acid enantiomers and microbial community at MOLA time series in the NW Mediterranean

Highlights

- Ship-based time series can be combined with remote sensing to close sampling gaps.
- Phytoplankton spring bloom occurs between February and May in NW Mediterranean Sea.
- Phytoplankton and river discharge affect the seasonality of L-DHAA concentrations.
- Accumulation of d-DHAA suggests bacterial processing of labile DOC in summer.
- DOM-microbe interactions are most apparent in lineages associated with blooms

Seasonality of amino acid enantiomers and microbial community at MOLA time series in the NW Mediterranean

Anabel von Jackowski [1], Nawal Bouchachi [1], Quentin-Boris Barral [2], Paul Labatut [3], Barbara Marie [1], Olivier Crispi [1], Karine Escoubeyrou [3], Charles-Hubert Paulin [3], Celine Dimier [4], Josephine Ras [5], Alexander Hayward [6], Eva Ortega Retuerta [1]

1-CNRS/Sorbonne Université, UMR7621 Microbial Oceanography Laboratory, Banyuls sur Mer, France
2-CNRS/Université de Toulouse, UMR5566 Laboratory of Space Geophysical and Oceanographic Studies, Toulouse, France
3-Oceanographic Observatory of Banyuls sur Mer (OOB), Banyuls sur Mer, France
4-CNRS/Sorbonne Université, Institut de la Mer de Villefranche (IMEV), Villefranche-sur-Mer, France
5-CNRS/Sorbonne Université, UMR 7093 Laboratoire d'Océanographie de Villefranche (LOV), Villefranche, France
6-Danish Meteorological Institute, København, Denmark

* Corresponding author:
Anabel von Jackowski vonjackowski@obs-banyuls.fr
Eva Ortega Retuerta, ortegaretuerta@obs-banyuls.fr

Keywords: Dissolved organic matter, phytoplankton, bacteria, amino acids, Mediterranean Sea

Abstract

Seasonality in light, temperature, and nutrient availability are well-known to regulate phytoplankton blooms and the bacterioplankton community. During the spring bloom, phytoplankton release biomolecules as part of the dissolved organic matter (DOM) pool exploited by the bacterioplankton. Here, we investigated the seasonal variability of phytoplankton biomass, enantiomers of dissolved hydrolyzable amino acids (DHAA), bacterioplankton abundances and community composition at the Microbial Observatory Laboratory Arago (MOLA) in the NW Mediterranean Sea from 2019 to 2021. Phytoplankton biomass estimated from pigment biomarkers suggests a spring bloom succession from cryptophytes, haptophytes, and prasinophytes in March to diatoms in April. The spring bloom coincided with a 50% increase in L-enantiomers of DHAA and an increase in bacterial abundance. After the spring bloom, elevated concentrations of D-enantiomers of DHAA and gamma-aminobutyric acid suggest bacterial processing of labile biomolecules contributed to the seasonal accumulation of dissolved organic carbon (DOC). Linking organic molecules with the free-living bacterioplankton community showed a seasonal succession of niches and substrate regimes. The parallel analysis of DOM and bacterioplankton community provides an important baseline for bacteria-substrate relationships over the seasonal cycle in the northwestern Mediterranean Sea.

1 Introduction

Marine dissolved organic matter (DOM) is a diverse mixture of compounds that account for 662 Pg of organic carbon and play a critical role in global biogeochemical cycles (Hansell, 2013). A single water sample can contain up to 20,000 molecular formulas, most of which remain uncharacterized to date (Riedel and Dittmar, 2014; Wagner et al., 2020). The characterizable fraction of DOM is frequently described based on its physical properties, i.e., size, and/or characterizing major biochemical groups, such as amino acids, to determine the bioavailability, diversity, and origin. Specifically, amino acids can be used to estimate the labile, semi-labile, and refractory DOC reservoirs (Davis and Benner, 2007).

DOM sources and sinks can be estimated using L- and D-enantiomers of amino acids. The main sources of marine DOM are phytoplankton biomass that produce L-enantiomers of amino acids, which are essential building blocks for all living organisms (Jørgensen et al., 1999). DOM is remineralized by heterotrophic bacterioplankton (i.e., archaea and bacteria), which are enriched in D-enantiomers as key constituents of the peptidoglycan, capsules, lipopolysaccharides, siderophores, and antimicrobial peptides (Park and Strominger, 1957; Hancock, 1960; Lam et al., 2009). Additionally, most bacterioplankton preferentially use L- over D-enantiomers of amino acids (Azúa et al., 2014; Zhang and Sun, 2014). Some cultural representatives do use D-amino acids, with a preference for D-Alanine, D-Glx, D-Asx, and D-Serine over D-Methionine, D-Valine, and D-Leucine, which are assumed to be less bioavailable (Zhang et al., 2016). Therefore, tracing the evolution of both pools of enantiomers in dissolved hydrolyzable amino acids

(DHAA) can provide information on whether the main DOM sources are phytoplanktonic versus bacterial origin.

DOM bioavailability varies seasonally and controls the bacterioplankton community. Organic carbon is predominantly derived from phytoplankton blooms that provide pulses of labile and semi-labile compounds, which sustain bacterial carbon and energy requirements during a given year (Piontek et al., 2011; Liu et al., 2020, 2022; von Jackowski et al., 2022). Upon the decay of the spring phytoplankton bloom, members of the *Roseobacter* clade (class: Alphaproteobacteria) and Flavobacteria (class: Bacteroidetes) typically dominate the bacterioplankton community in early successional stages (Pinhassi and Hagström, 2000; Teeling et al., 2016; Bunse and Pinhassi, 2017). In summer, SAR86 (class: Gammaproteobacteria) and SAR11 (class: Alphaproteobacteria) become dominant clades in the bacterioplankton community (Alderkamp et al., 2006; Alonso-Saez et al., 2007; Salter et al., 2015). Simultaneously, semi-labile DOM compounds tend to accumulate since they resist rapid bacterial turnover and possibly remineralized during fall or exported to the deep ocean during wintertime convective mixing (Carlson et al., 1994; von Jackowski et al., 2020).

In the NW Mediterranean Sea, abiotic factors control the seasonal niche preferences of the autotrophic and heterotrophic community (Salter et al., 2015; Galand et al., 2018; Lambert et al., 2019). Seasonal changes in the DOM pool are driven by the interplay between bacterioplankton during the spring bloom and low salinity water (LSW, PSU < 37.9) events in summer (Laghdass et al., 2010; Gonzalez et al., 2019). Additionally, the release of phytoplankton-derived transparent exopolymer particles (TEP) have been linked to a peak in bacterial

extracellular enzyme activities resulting in an accumulation of recalcitrant dissolved organic carbon (DOC) in the euphotic zone (0-200 m) during the summer stratification period (Copin-Montégut and Avril, 1993; Romera-Castillo et al., 2010; Vila-Reixach et al., 2012; Jones et al., 2013; Ortega-Retuerta et al., 2018). It is possible that the seasonal accumulation of recalcitrant DOC causes a malfunctioning of the microbial loop in summer to late fall (Thingstad et al., 1997; Sánchez-Pérez et al., 2020). To understand seasonal DOC accumulation and its factors in regulating bacterioplankton community patterns, we conducted a 3-year survey at the Microbial Observatory Laboratory Arago (MOLA) in the Gulf of Lion, northwestern Mediterranean Sea (NWMED). We hypothesized that the pronounced seasonal variability of DHAA regulates the bioavailability, which has consequences for microbial loop dynamics. Assessing relationships between microbes (i.e., phytoplankton and bacterioplankton) and the DOM pool over the seasonal cycle is important to understanding carbon cycling and substrate regimes in the NW Mediterranean Sea.

2 Material and Methods

2.1 *Sampling Site*

The "Microbial Observatory Laboratory Arago" (MOLA) time series station is located at the edge of the continental shelf in the NW Mediterranean Sea (42°27′205″N - 3°32′565″E) (Fig. 1). MOLA core parameters are sampled almost every month since 2004 and the time series was incorporated into the Mediterranean Ocean Observing System for the Environment (MOOSE) research infrastructure in 2010. At MOLA, the conductivity, temperature, and depth sensor

(CTD) is equipped with two temperature probes, two conductivity probes, and a Digiquarz pressure sensor. Seawater is collected using 12-L Niskin bottles to sample nine discrete depths: 5 m, 20 m, 40 m, 80 m, 120 m, 150 m, 200 m, 300 m, and 500 m.

MOLA was sampled 20 times for MOOSE core parameters and additional microbial parameters between 2019 and 2021 (Supplementary Table 1). In brief, MOOSE core parameters include the concentration of oxygen determined with titration (Winkler, 1888), inorganic nutrients determined on a continuous flow nutrient analyzer (AA3HR AutoAnalyzer, Bran-Luebbe, Ireland), chlorophyll-a (chl-a) extracted from GF/F filters (Whatman, USA) with acetone and determined fluorometrically (Evans et al., 1987), particulate organic carbon and nitrogen determined on a CHNS-O Elemental Analyzer (Sharp, 1974), and bacterial cell counts determined using flow cytometry (Cytoflex, Beckman Coulter, USA) and converted into abundances using the software FlowJo (v7.6, USA). The protocols for the core parameters and data management are available on the MOOSE website (https://www.moose-network.fr/). Additional microbial parameters included pigment-based chemotaxonomy, dissolved organic carbon (DOC), total dissolved nitrogen (TDN), total dissolved phosphorus (TDP), dissolved hydrolyzable amino acids (DHAA), and bacterioplankton community composition using the 16S rRNA marker gene.

2.2 Characterization of *DOM and Amino Acid Enantiomers*

Seawater for DOM was filtered through a double-layer of combusted GF/F filters (450°C for 8 hours, Whatman, USA), equivalent to 0.2 µm pore-size, and collected

at all MOLA depths between 5-500 m. Samples for DOC were fixed with 10 µL phosphoric acid (pH < 2), and measured using high-temperature catalytic oxidation (Sugimura and Suzuki, 1988; Qian and Mopper, 1996). Samples for TDN and TDP were submitted to persulfate wet-oxidation (Pujo-Pay and Raimbault, 1994) and using inorganic nutrients were then used to derive dissolved organic nitrogen and phosphorus (DON and DOP) concentration.

Samples for DHAA were collected at 5 and 500 m. Seawater was filtered through a double-layer of combusted GF/F filters (Whatman, USA) and collected in combusted glass vials and frozen (-20°C). Samples and blanks using ultrapure water were analyzed following the protocol by Escoubeyrou and Tremblay (2014). In brief, hydrolysis (110°C for 20 h) with hydrochloric acid (30% Suprapur, Merck Millipore, USA) under vacuum and o-phthaldialdehyde derivatization with either N-Isobutyryl-L-Cysteine (Sigma-Aldrich, USA) for the L-DHAA reagent run or N-Isobutyryl-D-Cysteine for D-DHAA reagent run separated enantiomeric amino acids and achiral amino acids by reversed-phase high-performance liquid chromatography (HPLC). The HPLC (UltiMate 3000, Thermo Fisher Scientific, USA) was equipped with a Gemini C18 column (Phenomenex, USA), an autosampler, and a fluorescence detector (excitation at 335 nm, emission at 450 nm). A gradient of the organic phase (methanol, acetonitrile) and phosphate buffer was used with a constant flow rate of 0.8 mL per minute (Escoubeyrou and Tremblay, 2014). DHAA identification and quantification in unknown samples were achieved by comparing the retention times and peak areas with those of standard amino acid solutions and procedural blanks were subtracted from final concentrations. Asparagine and Glutamine were deaminated during the

hydrolysis and were quantified as Aspartic acid (Asx) and Glutamic acid (Glx). Overall, 13 L-DHAA were detected: Alanine, Arginine, Asx, Glx, Histidine, Isoleucine, Leucine, Lysine, Phenylalanine, Serine, Threonine, Tyrosine, and Valine. A total of 6 D-DHAA were detected: Alanine, Asx, Glx, Leucine, Serine, and Valine. Additionally, we detected Beta-Alanine, Glycine, and Gamma-aminobutyric acid (GABA).

2.3 *Phytoplankton Pigment Analysis*

Seawater (1-2 L) for pigment-based chemotaxonomy was collected at 5 m, filtered onto combusted GF/F filters (Whatman, USA), and stored frozen (-20°C). The filters were extracted using 3 mL methanol (100%) for two hours, disrupted by sonication, and clarified by vacuum filtration through GF/F filters. The extracts were quantified using reversed-phase HPLC (Agilent Technologies, USA), after Ras et al. (2008). Phytoplankton taxonomy was assessed from pigment concentrations (Table 1) and converted into class abundances and pigment-to-chl-a ratios (Supplementary Table 2) using r-package "phytoclass" (v.1.0.0) (Hayward et al., 2023) that is based on CHEMTAX program (Mackey et al., 1996).

Table 1. List of the pigments used in this study and their taxonomic significance (Roy et al., 2011).

Chlorophylls	**Taxonomic or biochemical significance**
Alloxanthin	Cryptophytes
Bacteriochlorophyll-a	Photoheterotrophic bacteria
Chlorophyll-b	Chlorophytes, Prasinophytes
19-Butanoyloxyfucoxanthin	Haptophytes, Pelagophytes

Fucoxanthin	Diatoms, Haptophytes, some Dinoflagellates, Pelagophytes
19-Hexanoyloxyfucoxanthin	Haptophytes
Lutein	Chlorophytes, Prasinophytes,
Neoxanthin	Prasinophytes, Chlorophytes
Peridinin	Dinoflagellates
Prasinoxanthin	Prasinophytes
Violaxanthin	Chlorophytes, Prasinophytes
Zeaxanthin	Cyanobacteria, Chlorophytes, Prasinophytes, Flavobacteria

2.4 *Bacterioplankton Community Analysis*

Samples for genomic DNA were collected at 5 and 500 m. Around 5 L of seawater was filtered through 3.0-µm and then 0.22-µm filters (Nucleopore, USA) using a peristaltic pump and stored frozen (-80°C). The genomic DNA was lysed with lysozyme (20 mg mL^{-1}, 45 min at 37°C, Sigma-Aldrich, USA), proteinase K (20 mg mL^{-1}, 60 min at 55°C, Sigma-Aldrich, USA), and extracted using Zymobionics DNATM Miniprep Kit (Cat. No.: D6005, Zymo Research, USA). PCR-amplification using the universal 16S rRNA 515F and 926R primer pair covering the v4-v5 hypervariable region (Parada et al., 2016) and sequenced on a MiSeq platform (Illumina, USA) at LGC Genomics GmbH (Berlin, Germany).

Amplicon reads were processed in RStudio (v2023.09.1+). FastQ files were processed into amplicon sequence variants (ASVs) using the R-package 'dada2' (v1.16.1) (Callahan et al., 2016). Filtering settings were truncLen=c(190,200), maxN=0, minQ=2, maxEE=c(3,3) and truncQ=0, followed by merging using

minOverlap=10 and chimera removal. After singleton removal, we obtained an average of 53,387 reads per sample. ASVs were taxonomically classified using the SILVA SSU Reference dataset (release v138.1) (McLaren and Callahan, 2021). ASVs with less than three counts in less than 3% of samples were excluded. ASVs were further analyzed using R-packages 'phyloseq' (v1.42.0) (McMurdie and Holmes, 2013), 'ampvis2' (v2.8.3) (Andersen et al., 2018), and 'microeco' (v1.4.0) (Liu et al., 2021).

2.5 *Statistical Analyses*

Data processing and statistical analyses were conducted in RStudio (v2023.09.1+). Statistical analyses focused on changes within a Julian year, since the sampling gaps over the course of the three-year time series made it inapt to determine monthly averages or inter-annual variation within the discrete variables.

For all environmental parameters, arithmetic means and standard deviations were calculated using the 'base' package (v4.2.1) and Spearman correlations were corrected using a false discovery rate (FDR) adjusted p-value (also called q-value) of 0.05. Degradation indices of DHAA were calculated based on Kaiser and Benner (2009) by summarizing L- and D-enantiomer concentrations. Integrations of the upper 500 m were performed using trapezoidal integration.

For the amplicon data, alpha-diversity was analyzed with 'iNEXT' (v3.0.0) (Hsieh et al., 2016) and permutational multivariate analysis of variance (PERMANOVA) were calculated using vegan ('adonis2' and 'vegdist' functions, v2.6.4) (Oksanen et al., 2022). Log_2fold-change (log_2FC) had an adjusted p-value

of 0.05 using the 'DESeq2' (v1.38.3) (Love et al., 2014) to investigate the differences in bacterioplankton community between the free-living (FL) and particle-attached (PA) size fractions. Distance-based redundancy analysis (dbRDA) was fit with significant environmental vectors using vegan ('envfit' function) to investigate seasonal environmental drivers of FL bacterioplankton community at 5 m (Buttigieg and Ramette, 2014). Similarly, Pearson correlations with an FDR-adjusted p-value was performed between ASVs and the environmental data using 'microeco' (function 'cal_cor', v1.4.0) to investigate drivers of taxa (Liu et al., 2021).

Visualizations were performed in MATLAB with M_Map (Pawlowicz, 2020) and using R-package ggplot2 (v3.4.3) (Wickham, 2016). All scripts are publicly available via https://github.com/anabelvonjackowski/.

2.6 *Remote Sensing and Simulation Approaches*

Remote sensing data products were used to fill in the gaps between discrete sampling events of temperature, salinity, and chl-*a* at MOLA. For sea surface temperature (SST), L4 satellite data was downloaded from the Copernicus Marine Environment Monitoring Service (CMEMS), resulting in a high-resolution dataset (VHR, 1/40°, ~1.4 km) of daily SST averages (Buongiorno Nardelli et al., 2013).

For salinity, we used two remote sensing data products to fill in the gaps between discrete sampling events. Sea surface salinity (SSS) lacks a high-resolution satellite-derived data for the Mediterranean (SSS, > 30 km with the SMOS satellite) (Olmedo et al., 2018) and artifacts (>40) in global ocean datasets. Consequently, we chose to apply two simulations with assimilations of observations: a reanalysis for the January 2019 to June 2021 period and an

operational model from August to December 2021 to finalize the time series. The high resolution (1/24°, ~4 km) of the daily reanalysis (Escudier et al., 2021), the daily CMEMS analysis, and the forecast model (Clementi et al., 2019) allowed the assimilation of *in situ* temperature and salinity vertical profiles and satellite sea level anomaly along the track data through an OceanVar assimilation scheme.

For sea surface chl-*a*, mass concentration data was downloaded from the L4 CMEMS satellite-derived product at 1km resolution (Berthon and Zibordi, 2004; Volpe et al., 2018, 2019). The data was reconstructed using satellite-merged (SeaWiFS, MODI, MERIS, VIIRS-SNPP & JPSS1) bio-optical multi-sensors that use empirical and semi-analytical algorithms to calculate the remotely sensed chl-*a*. Daily outputs were reprocessed with climatological data for the smoothing procedure of the sensor merging, in addition with the DINEOF (Data INterpolating Empirical Orthogonal Functions) algorithm to fill in missing data due to cloud cover. Since oligotrophic waters of the Mediterranean are greener and less blue than other ocean basins, the algorithm parameterized at a regional level (an updated version of MedOC4) provides a more accurate estimate compared to the overestimated chlorophyll by the global algorithm. Furthermore, algorithm assessment and validation concluded that the product is in good agreement with historical in situ chlorophyll data.

3 Results

Discrete sampling and remote-sensing approaches showed well-defined seasonal patterns in temperature and salinity. The *in situ* surface (5 m) temperatures ranged from 13 to 24°C (n=20), while satellite-derived sea surface temperatures

(SST) ranged between 13 to 25°C (n=1096) with rapid increases from ~15°C in May to >18°C in June 2019 and 2021 compared to ~15°C in April to >18°C in June in 2020. The *in situ* surface salinity ranged from 37.7 to 38.2 PSU (n=20), while satellite-derived sea surface salinity (SSS) ranged between 37.5 and 38.4 PSU (n=1057), both suggesting the occurrence of LSW (PSU < 37.9, >3 days) events but with inter-annual variability between 2019 to 2021. LSWs likely ranged from 17 June to 29 July 2019, 09 June to 21 July 2020, and 28 May to 28 June 2021 (Fig. 1c). At 500 m, temperatures remained ~14°C and salinity ~39 PSU (n=5) year-round, but data are only available for 2021.

The remote-sensing approach confirmed that spring bloom in the NWMED occurred between February and May. Satellite-derived sea surface chl-*a* ranged from 0.05 to 0.60 µg L^{-1} (n=1096), which was slightly lower than the *in situ* surface chl-*a* that ranged from 0.07 to 1.0 µg L^{-1} (n=21; Fig. 1c). Both satellite-derived and *in situ* chl-*a* show inter-annual variability in bloom dynamics between 2019 to 2021. Discrete measurements of chl-*a* increased by 85% from February to March before declining 37% from March to April until the beginning of the new productive season in November (Fig. 1c). Phytoplankton taxonomy estimated from pigment biomarkers suggests that the spring bloom was dominated by cryptophytes, haptophytes, and prasinophytes at the beginning of March and diatoms in early February as well as the end of April (Fig. 2a). Accordingly, chl-a showed significant positive correlations with cryptophytes ($r=0.83$, $p<0.001$), haptophytes ($r=0.84$, $p<0.001$), prasinophytes ($r=0.88$, $p<0.001$), dinoflagellates ($r=0.86$, $p<0.001$), and diatoms ($r=0.63$, $p=0.01$, Supplementary Fig. 1). Chlorophytes were only observed

in spring 2021, while *Synechococcus* appeared to grow in spring, summer, and fall (Fig. 2a and 3).

Maximal inorganic nutrient concentrations were observed in winter, which gradually decreased during the productive season until late fall. At 5 m, nitrate (NO_3-) ranged from below the detection limit to 2.3 μmol L^{-1} (n=21), nitrite (NO_2-) ranged from 0.010 to 0.25 μmol L^{-1} (n=21), and silicate (SiO_4) ranged from 0.25 to 2.0 μmol L^{-1} (n=21). Ammonium (NH_4+) ranged from below the detection limit to 0.068 μmol L^{-1} (n=21), and phosphate (PO_4^3-) ranged from 0.010 to 0.80 μmol L^{-1} (n=21). At 500 m, NO_3- ranged from 7.7 to 9.1 μmol L^{-1} (n=18), NO_2- ranged from 0.010 to 0.31 μmol L^{-1} (n=18), PO_4^3- ranged from 0.31 to 0.41 μmol L^{-1} (n=18), and SiO_4 ranged from 5.1 to 7.6 μmol L^{-1} (n=18).

Maximal POC concentrations and minimum DON concentrations were observed in winter, while DOC and DOP concentrations decreased to a minimum spring and accumulated during the productive season. At 5 m, concentrations of POC ranged from 4.1 to 19 μmol L^{-1} (n=21) and generally decreased from winter and throughout the productive season until fall (Supplementary Fig. 2). DOC ranged from 58 to 102 μmol L^{-1} (n=21), DON concentrations ranged from 4.5 to 7.6 μmol L^{-1} (n=19), and DOP concentrations ranged from 0.038 to 0.13 μmol L^{-1} (n=19; Supplementary Fig. 2). DOC:DON:DOP ratios increased from 13:92:1 in spring, 14:96:1 in summer, 15:68:1 in fall, and decreased to 15:77:1 in winter. DOC significantly negatively correlated with chl-*a* (r=-0.59, p<0.001). At 500 m, POC concentrations ranged from 1.8 to 16 μmol L^{-1} (n=20) or 1529 to 4733 mmol m^{-2} and peaked in winter and late summer (n=20; Supplementary Fig. 3). DOC concentrations ranged from 45 to 94 μmol L^{-1} (n=18), DON ranged from 2.8 to 5.9

295 μmol L^{-1} (n=18), and DOP ranged from below the detection limit to 0.13 μmol L^{-1}
296 (n=18; Supplementary Fig. 3).

297 DHAA concentrations showed seasonal variability with an accumulation of
298 L-DHAA in March and July compared to a gradual accumulation of D-DHAA until
299 late summer. At 5 m, DHAA ranged from 0.65 to 1.17 μmol L^{-1} (n=13) that
300 negatively correlated with salinity (r=-0.62, p<0.05) and diatoms (r=-0.82, p<0.01).
301 Calculating degradation indices (DI) showed positive DIs (less degraded) in spring
302 and during the LSW events in June compared to negative DIs (more degraded) in
303 winter (Fig. 2b). Further investigating the enantiomer composition showed that
304 L-DHAA ranged from 0.38 to 0.67 μmol L^{-1} (n=13; Fig. 2c) and significantly
305 negatively correlated to diatoms (r=-0.77, p<0.01; Supplementary Fig. 1). In
306 contrast, D-DHAA ranged from 40 to 68 nmol L^{-1} (n=15; Fig. 2c) and significantly
307 increased with the Julian Day (JD) (r=0.72, p=0.0025), while significantly
308 negatively correlating with chl-a (r=-0.69, p<0.01) and phytoplankton groups that
309 bloomed in March (Supplementary Fig. 1). Specifically, individual monomers
310 showed that all L-DHAA increased more than two-fold from February to March
311 (Fig. 2d), while several L-DHAA (Histidine, Lysine, Serine, Tyrosine, and Valine)
312 decreased more than 1.3-fold in April (Fig. 2e). Similar to their L-DHAA
313 counterparts, B-Alanine, D-Alanine, and D-Glx also increased in April, whereas
314 D-Serine and D-Valine decreased in April (Fig. 2f). Generally, B-Alanine and D-
315 DHAA increased throughout the year (Fig. 2f). At 500, DHAA ranged from 0.42 to
316 4.6 μmol L^{-1} with L-DHAA ranging from 0.17 to 1.7 μmol L^{-1} (n=15) peaking in
317 spring and D-DHAA ranging from 27 to 142 nmol L^{-1} (n=15) increasing towards
318 fall (Supplementary Fig. 3).

Seasonal changes were observed in the bacterioplankton abundance and community composition at 5 m. Bacterioplankton abundances ranged from 3.8 to 13 x10^5 cells mL^{-1} (n=20) with a notable shift in high (HNA) and low nucleic acid (LNA) subgroups. HNA cells ranged from 1.8 to 5.2 x10^5 cells mL^{-1} (n=20) and peaked in late February to May and July to September. LNA cells ranged from 1.6 to 8.9 x10^5 cells mL^{-1} (n=20) and peaked in late February to early March and July to August (Supplementary Fig. 2). Assessing the amplicon data showed that the sequencing depth sufficiently covered the bacterioplankton diversity free-living (FL) fraction and particle-attached (PA) ~99.7% (Supplementary Fig. 4). At 5 m, the FL community significantly changed with the JD (PERMANOVA, $p<0.01$) along with the PA community that also significantly changed with the JD (PERMANOVA, $p<0.05$; Supplementary Table 3). Furthermore, alpha-diversity indices of the FL showed a significant increase in richness ($r=0.69$, $p=0.0041$) and Shannon diversity ($r=0.52$, $p=0.045$) with the JD (Supplementary Fig. 5, outlier JD 27). At the class level, FL and PA were represented by Alphaproteobacteria, Gammaproteobacteria, Bacteroidetes, and Cyanobacteria up to 80%. At the family level, FL community was dominated by SAR11 clade I ~18.8%, SAR11 clade II ~6.2%, and Flavobacteriaceae ~12.8% year-round, while Cyanobiaceae showed monthly fluctuations. The PA community was dominated by Cyanobiaceae ~21.7% and families in Bacteroidetes ~19.8% but also reoccurring Pirellulaceae ~2.8%, Puniceicoccaceae 2.6%, and Vibrionaceae ~3.5% (Fig. 3). Testing the seasonal enrichment showed significant changes in SAR11 clades, SAR86 clade, and AEGEAN-169 marine group during spring, summer, or winter in FL (log_2FC

342 q<0.001) compared to Planctomycetes in winter in PA (log_2FC q<0.001,
343 Supplementary Fig. 6).

344 Seasonal changes were less pronounced in the bacterioplankton abundance
345 and community composition at 500 m. Bacterial abundances ranged from 0.97 to
346 9.6 x10^5 cells mL^{-1} (*n*=19) with HNA ranging from 0.48 to 5.1 x10^5 cells mL^{-1} (*n*=19)
347 and LNA ranged from 0.47 to 4.5 x10^5 cells mL^{-1} (*n*=19). Assessing the amplicon
348 data showed that the sequencing depth sufficiently covered the bacterioplankton
349 diversity FL fraction and PA ~99.3% (Supplementary Fig. 4). The alpha-diversity
350 indices gradually decreased by JD in the FL, while alpha-diversity peaked in
351 summer within the PA (Supplementary Fig. 5). At the class level, the FL was
352 dominated by Nitrososphaeria, whereas the PA community had representatives of
353 Alphaproteobacteria, Gammaproteobacteria, Bacteroidetes up to 50% (Fig. 3). At
354 family level, FL community was dominated by Nitrosopumilaceae ~32.3% along
355 with SAR11 clades I ~8.5% and clade II ~4.7%. PA community was almost year-
356 round, represented by Nitrosopumilaceae, Pirellulaceae, Crocinitomicaceae, and
357 Phycisphaeraceae ~4%.

358 Combining environmental parameters with the FL bacterioplankton
359 community suggests DOM-microbe interactions. A distance-based redundancy
360 analysis (dbRDA) was used to assess the influence of environmental explanatory
361 variables (arrows) on the ASV abundance data. At 5m, the dbRDA showed that
362 salinity, dinoflagellates, and pelagophytes significantly constrained the ordination
363 space of the response variables (points) corresponding to the winter and spring
364 samples (p<0.05, Fig 4a). In contrast, temperature, D-Asx, and DON significantly
365 constrained the ordination space corresponding to summer and fall (p<0.05, Fig.

4a). Attempting direct links between environmental parameters and the FL bacterioplankton community showed that *Candidatus* Nitrosopumilus and common bloom-associated genera within the Roseobacter lineage and Flavobacteriaeae positively correlated with phytoplankton groups, while negatively correlating with temperature (p-adj<0.05; Fig. 4b). In contrast, genera such as *Candidatus* Aquiluna, *DS001*, and other Roseobacter group members positively correlated to several L-DHAA (p-adj<0.05, Fig. 4b). At 500 m, data were insufficient to derive the significant environmental variables, but L-DHAA constrained the ordination space corresponding to winter samples, while DON, DOP, and D-DHAA constrained the ordination space of summer and fall samples (Supplementary Fig. 7). Direct links were limited in the mesopelagic depth with few genera showing significant links to L-DHAA, B-Alanine, and D-Serine (Supplementary Fig. 7).

4 Discussion

4.1 The spring bloom in the NWMED

The haptophyte- and diatom-dominated blooms caused L-DHAAs and the degradation index to peak at 5 m during spring (Fig. 2). The phytoplankton spring bloom composition at MOLA was similar to nearby coastal time series *Service Observation Laboratory Arago* (SOLA), *Blanes Bay* near Barcelona, Spain, and *DYFAMED* near Villefranche-sur-Mer, France (Marty et al., 2002; Latasa et al., 2010; Gutiérrez-Rodríguez et al., 2011; Nunes et al., 2018). However, relative abundances of *Synechococcus* were higher at MOLA compared to the Adriatic Sea (Trano et al., 2022). The increase of phytoplankton-derived L-DHAA could be

similar across the NWMED with a release of hydroxyl-amino acids (L-Serine and L-Threonine) and glycine from diatom cell walls post-bloom in March (Hecky et al., 1973; Dauwe and Middelburg, 1998). In June, the peak of aromatic-DHAA (L-Phenylalanine and L-Tyrosine) and L-Asx might have been released by cell exudation or lysis of diatoms (Hecky et al., 1973). Furthermore, the different pattern of L-Glx, which was low during the first diatom bloom but increased to 135 nmol L^{-1} during the second diatom bloom in April, might suggest a succession of diatom populations. *Chaetoceros* sp. and *Rhizosolenia* sp. tend to bloom in early spring, while *Pseudo-nitzschia* sp. has been observed to bloom at SOLA between March and May (Charles et al., 2005; Quiroga, 2006). Overall, chl-*a* and L-DHAA concentrations were over 2-fold higher in surface waters at MOLA compared to more oligotrophic sites during spring and summer, such as Bermuda Ocean Time Series Station (BATS) and Hawaii Ocean Time Series (HOT) (Lomas et al., 2013; Wirtz and Smith, 2020; Ianiri et al., 2022). Studying phytoplankton bloom dynamics is essential to understand biogeochemical and microbial interactions. We strongly encourage time series to analyze larger phytoplankton via microscopy or automated imaging systems, e.g., imaging flow cytobot (IFCB) (Olson and Sosik, 2007; Sosik and Olson, 2007), and additional sampling efforts for smaller phytoplankton, e.g., flow cytometry, to better understand the mechanisms of bloom formation and links to biochemistry at offshore time series.

DOM bioavailability positively correlated with bacterial abundances and coincided with copiotroph ecological strategies. Heterotrophs can be generally distinguished as either HNA or LNA, where HNA are considered to be a more substrate-driven and metabolically active subpopulation than LNA (Robertson

414 and Button, 1989; Sherr et al., 2006; Bouvier et al., 2007). Furthermore,
415 heterotrophs can be distinguished as either copiotrophs that compete under high
416 DOM concentrations or oligotrophs adapted to low concentrations (Koch, 2001;
417 Giovannoni et al., 2014). In terms of composition, Bacteriodetes (Flavobacteriacae)
418 and members of the *Roseobacter* group are non-seasonal and known copiotroph
419 bacteria since they are more competitive under bioavailable DOM levels in the
420 NWMED (Lambert et al., 2019; Auladell et al., 2022). The positive correlations
421 with phytoplankton groups are indicative of labile DOM and diatom-derived DOM
422 consumption (Sarmento et al., 2013; Landa et al., 2018). Alongside the
423 copiotrophs, we find oligotrophs such as SAR11 (Fig. 3). Within SAR11, the
424 ecotype-like clades exhibit pronounced seasonal cycles and confirm previous
425 observations that SAR11 clade *Ib* is associated with replete nutrient
426 concentrations and phytoplankton biomass, while clade *Ia* are adapted to thrive
427 under basal DOM levels (Salter et al., 2015). SAR11 ecotypes appear to be
428 differentially involved in the labile and humic substrate processing during the
429 spring bloom and can not be classified into these over-simplified ecological
430 strategies (Malmstrom et al., 2004; Alonso-Sáez and Gasol, 2007; Laghdass et al.,
431 2012). Still, a bacterioplankton community with fairly balanced proportions of
432 copiotrophs and oligotrophs can simultaneously process the phytoplankton-
433 derived protein-like substances that contribute to the labile DOC pool and humic-
434 like fluorescent organic matter that contribute to the recalcitrant DOC pool
435 released during the spring bloom (Yamashita and Tanoue, 2003; Romera-Castillo
436 et al., 2010; Sánchez-Pérez et al., 2020). Furthermore, experiments have shown
437 that picocyanobacteria and bacterioplankton produce humic-like fluorescent

organic matter under phosphorus-replete conditions during the spring bloom (Romano et al., 2014; Zhao et al., 2017; Bouchachi et al., 2023). The humic-like fluorescent organic matter would be less bioavailable than phytoplankton-derived compounds and possibly serve oligotrophs. Overall, the copiotrophs appear to be processing labile DOM, like *Roseobacter*, while oligotrophs might be processing relatively refractory DOM, like SAR11 clade *Ia*, and supports the notion that trophic strategies follow a gradient from copiotrophy to oligotrophy at the end of spring (Lemonnier et al., 2020).

4.2 Microbial loop dynamics from summer until winter

LSWs are diluted mesoscale structures that detach from the Rhône River plume to the open Mediterranean Sea and impact biogeochemical processes around June to July each year (Diaz et al., 2008). Our study confirms that LSWs are low in chl-a and dissolved inorganic nitrogen (DIN) but contain bioavailable DOM that sustains bacterial activity (Laghdass et al., 2010; Gonzalez et al., 2019). In 2020, we observed a strong increase in several L-DHAA and DI, therefore bioavailability, during the LSW (JD 175) compared to after the LSW (JD 203; Fig. 2). Enrichments of phenylalanine and valine could have been released from *Chaetoceros* sp. (Poulet and Martin-Jézéquel, 1983; Sarmento et al., 2013). Isoleucine and leucine are known to contribute to the highly labile fraction of DOM (Carlson and Ducklow, 1995; Cherrier et al., 1996), promoting bacterioplankton growth in summer.

Bacterioplankton were increasingly exposed to D-DHAA towards fall (Fig. 2). DHAA accumulated on the surface waters during summer, which appeared as

462 relatively short-term fluctuations in individual L-DHAA but a steady increase of
463 D-DHAA concentrations until fall (Fig. 2). Since D-DHAA amino acids are proxies
464 of bacterial-derived DOM, their presence indicates more degraded DOM at the end
465 of the accumulation period. To further understand the accumulation in the D-
466 DHAA pool, "canonical" DHAA (D-Alanine, D-Asx, D-Glx) showed relatively
467 higher concentrations and greater seasonal variability than "non-canonical"
468 DHAA (D-Leucine and D-Valine; Fig. 2), which is similar to previous observations
469 (Broek et al., 2019; Ianiri et al., 2022). Canonical DHAA are more abundant in the
470 HMW material and non-canonical DHAA are more abundant in the LMW material
471 (Ianiri et al., 2022), which could suggest a preference of bacterioplankton for
472 canonical D-DHAA. For example, D-Alanine is a key component of autotrophic and
473 heterotrophic bacterial peptidoglycan (Schleifer and Kandler, 1972; Kaiser and
474 Benner, 2008; Cava et al., 2011), which would be relatively rapidly remineralized
475 compared to recalcitrant DHAA that accumulates as part of the LMW DON
476 towards fall (Ianiri et al., 2022). Nonetheless, D-DHAA can be used as a nitrogen
477 source for bacterial growth, to modulate cell wall biogenesis or act as a chemotactic
478 warning signal, but many of the related functions and metabolic pathways remain
479 unknown (Zhang et al., 2016; Yu et al., 2020; Irazoki et al., 2023). The seasonal
480 changes in the DHAA pool amid few correlations to the bacterioplankton
481 community (Fig. 4) highlight the complex interactions among the abiotic and biotic
482 factors in the microbial loop. More research with longer sampling frequencies of
483 time series-based studies and higher resolution of 'omic approaches (e.g., meta-
484 and transcriptomics) are needed to better unravel the interactions between the

485 composition of the amino acid pool and microbial communities in the NW
486 Mediterranean.
487
488 ***4.3 Mesopelagic DOM-Bacterioplankton interactions***
489 Organic matter seasonal variations in euphotic and mesopelagic zones will affect
490 the deep ocean bacterioplankton community and their metabolism. In MOLA,
491 mesopelagic POC and L-DHAA concentrations peaked during the spring and
492 summer, while D-DHAA concentrations remained fairly constant at depth
493 (Supplementary Fig. 3). In comparison, individual and total L-DHAA
494 concentrations were over 2-fold higher at MOLA than previously reported from
495 more oligotrophic sites during spring and summer, such as BATS and HOT (Kaiser
496 and Benner, 2008; Ianiri et al., 2022). The enrichment of L-DHAA at MOLA could
497 be due to a reduced DHAA degradation since bacterial production, which is around
498 2-3 times lower at the bottom of the euphotic zone relative to BATS (Gonzalez et
499 al., 2019; Liu et al., 2022). Alternatively, the elevated chl-*a* at the surface relative
500 to previous observations (section 4.1) could have enhanced organic matter export
501 at MOLA through various pathways (phytoplankton, aggregates zooplankton
502 migration or mixing processes (Siegel et al., 2016; Le Moigne, 2019). Surface
503 productivity combined with strong continental (westerly/northerly) winds that
504 cause dense shelf water cascading events favor POC export in the southwestern
505 Gulf of Lyon, near MOLA (Puig et al., 2008; Sanchez-Vidal et al., 2008; Many et
506 al., 2021). Furthermore, assuming that sinking or ascending particles contributed
507 to the POC pool at MOLA, these sinking particles release amino acids into the
508 surrounding water (Smith et al., 1992; Grossart and Ploug, 2000; Baumas et al.,

2023). Finally, our 500m samples are taken near the seafloor, where sediment resuspensions into the nepheloid layer could have also been a source of L-DHAA. The diverse pool of available organic substrates shapes the diverse community across the different fractions in mesopelagic and relative to the euphotic zone (Ghiglione et al., 2012; Wilson et al., 2017; Baumas et al., 2021; Sebastián et al., 2021). We encourage future studies and time series that measure microbial variables to observe organic matter degradation, aggregation, and sinking in the meso- and bathypelagic zones since anthropogenic climate change affects the entire water column (Buttigieg et al., 2018; González-Dávila and Santana-Casiano, 2023; Baumas and Bizic, 2024).

5 Conclusion

Our assessment of the DOM pool and links to the phyto- and bacterioplankton communities revealed a seasonality in the surface waters and mesopelagic zone. In the surface, springtime phytoplankton blooms released L-DHAA, which increased HNA bacteria abundances and lowered alpha-diversity, thereby promoting bacterioplankton with copiotroph ecological strategies. A notable input of bioavailable DOC occurred during LSW events during summer. During summer, the accumulation of DOC and D-DHAA, the presence of LNA bacteria, and declining richness suggest that a broader community of less active bacterioplankton target more refractory substrates into fall. Our study highlights the seasonal variation in L- and D- enantiomers of DHAA and possible associations with the microbial community. We strongly encourage microbial time series observatories to incorporate or expand the range of discrete parameters to

incorporate biochemical measurements, such as DHAA, as tracers of bacterial molecules in the DON pool.

CRediT authorship contribution statement. Anabel von Jackowski: Data curation, Formal analysis, Visualization, Writing – original draft, Writing – review & editing. Nawal Bouchachi; Conceptualization, Investigation, and Data Curation. Quentin-Boris Barral; Methodology, Software, and Visualization. Paul Labatut: Investigation. Barbara Marie: Investigation and Formal analysis. Olivier Crispi: Investigation and Formal analysis. Karine Escoubeyrou: Investigation and Formal analysis. Charles-Hubert Paulin: Investigation and Formal analysis. Celine Dimier: Investigation and Formal analysis. Josephine Ras: Investigation and Formal analysis. Alexander Hayward: Software. Eva Ortega Retuerta: Conceptualization, Validation, Investigation, Resources, Writing – original draft, Writing – review & editing, Supervision, Project administration, Funding acquisition.

Acknowledgments. We thank the captain and the crew of the R/V NEREIS II for their support aboard in sample collection. We are grateful to Christophe Salmeron and David Pecqueur at the Biology Platform of Imaging and flow Cytometry (BioPIC) platform and the Biodiversity and Marine Biotechnologies (Bio2Mar) platform of the Oceanology Observatory of Banyuls-sur-Mer (OOB). We are also grateful to the SAPIGH platform of the Institut de la Mer de Villefranche (IMEV). This study used the European Union Copernicus Marine Service Information for remotely sensed sea surface temperature, sea surface chlorophyll-a, and simulated sea surface salinities came from CMEMS (Copernicus Marine Environment Monitoring Service). We thank the two anonymous reviewers for their time and effort that was put into reviewing the publication.

Funding. Anabel von Jackowski was funded by the French National Research Agency Project MicroPump (ANR-20-CE01-0007). Nawal Bouchachi was funded by the Ecole Doctorale 129 from Sorbonne University. This work was funded by National Institute for Earth Sciences and Astronomy (ODISEA, LEFE/CYBER 2019), and MicroPump (French National Research, ANR-20-CE01-0007) projects to Eva Ortega-Retuerta.

Conflict of interest. The authors declare no conflict of interest.

Data Availability, Products, and Datasets. Environmental data for DOM, DHAA enantiomers, and pigments are uploaded to PANGAEA under the accession number 967436 (von Jackowski et al., 2024). Raw fastq files have been deposited at ENA under accession number PRJEB75023.

- Mediterranean Sea - High Resolution And Ultra High Resolution Sea Surface Temperature Analysis, E.U. Copernicus Marine Service Informa-tion product [Data set]. Available at:
- https://resources.marine.copernicus.eu/?option=com_csw&view=details&product_id=SST_MED_SST_L4_NRT_OBSERVATIONS_010_004 (Accessed: September 2023)

- Mediterranean Sea, Bio-Geo-Chemical, L4, monthly means, daily gapfree and climatology Satellite Observations (1997-ongoing), E.U. Copernicus Marine Service Informa-tion product [Data set]. Available at:
- https://data.marine.copernicus.eu/product/OCEANCOLOUR_MED_BGC_L4_MY_009_144/ (Accessed: September 2023)
- Mediterranean Sea Physics Reanalysis, E.U. Copernicus Marine Service Informa-tion product [Data set]. Available at:
- https://data.marine.copernicus.eu/product/MEDSEA_MULTIYEAR_PHY_006_004 (Accessed: September 2023)
- Mediterranean Sea Physics Analysis and Forecast, E.U. Copernicus Marine Service Informa-tion product [Data set]. Available at:
- https://data.marine.copernicus.eu/product/MEDSEA_ANALYSISFORECAST_PHY_006_013 (Accessed: September 2023)

Documentations:

- Buongiorno Nardelli B., C.Tronconi, A. Pisano, R.Santoleri, 2013: High and Ultra-High resolution processing of satellite Sea Surface Temperature data over Southern European Seas in the framework of MyOcean project, Rem. Sens. Env., 129, 1-16, https://doi.org/10.48670/moi-00172
- Berthon, J.-F., Zibordi, G.: Bio-optical relationships for the northern Adriatic Sea. Int. J. Remote Sens., 25, 1527-1532, 2004, https://doi.org/10.1080/01431160310001592544
- Volpe, G., Buongiorno Nardelli, B., Colella, S., Pisano, A. and Santoleri, R. (2018). An Operational Interpolated Ocean Colour Product in the Mediterranean Sea, in New Frontiers in Operational Oceanography, edited by E. P. Chassignet, A. Pascual, J. Tintorè, and J. Verron, pp. 227–244, https://doi.org/10.17125/gov2018.ch09
- Volpe, G., Colella, S., Brando, V. E., Forneris, V., Padula, F. L., Cicco, A. D., ... & Santoleri, R. (2019). Mediterranean ocean colour Level 3 operational multi-sensor processing. Ocean Science, 15(1), 127-146, https://doi.org/10.5194/os-15-127-2019
- Escudier, R., Clementi, E., Cipollone, A., Pistoia, J., Drudi, M., Grandi, A., Lyubartsev, V., Lecci, R., Aydogdu, A., Delrosso, D., Omar, M., Masina, S., Coppini G., Pinardi, N. (2021). A High Resolution Reanalysis for the Mediterranean Sea. Frontiers in Earth Science, 9, 1060, https://www.frontiersin.org/article/10.3389/feart.2021.702285
- Clementi, E., Aydogdu, A., Goglio, A. C., Pistoia, J., Escudier, R., Drudi, M., Grandi, A., Mariani, A., Lyubartsev, V., Lecci, R., Cretí, S., Coppini, G., Masina, S., & Pinardi, N. (2021). Mediterranean Sea Physical Analysis and Forecast (CMEMS MED-Currents, EAS6 system) (Version 1) [Data set]. Copernicus Monitoring Environment Marine Service (CMEMS), https://doi.org/10.25423/CMCC/MEDSEA_ANALYSISFORECAST_PHY_006_013_EAS8

References

Alderkamp, A., Sintes, E., Herndl, G., 2006. Abundance and activity of major groups of prokaryotic plankton in the coastal North Sea during spring and summer. Aquatic Microbial Ecology 45, 237–246.

Alonso-Saez, L., Balagué, V., Sã, E.L., Sanchez, O., Gonzalez, J.M., Pinhassi, J., Massana, R., Pernthaler, J., Pedros-Alio, C., Gasol, J.M., 2007. Seasonality in bacterial diversity in north-west Mediterranean coastal waters: assessment through clone libraries, fingerprinting and FISH: Seasonality in marine bacterial diversity. FEMS Microbiology Ecology 60, 98–112.

Alonso-Sáez, L., Gasol, J.M., 2007. Seasonal Variations in the Contributions of Different Bacterial Groups to the Uptake of Low-Molecular-Weight Compounds in Northwestern Mediterranean Coastal Waters. Applied and Environmental Microbiology 73, 3528–3535.

Andersen, K.S., Kirkegaard, R.H., Karst, S.M., Albertsen, M., 2018. ampvis2: an R package to analyse and visualise 16S rRNA amplicon data. doi:10.1101/299537

Auladell, A., Barberán, A., Logares, R., Garcés, E., Gasol, J.M., Ferrera, I., 2022. Seasonal niche differentiation among closely related marine bacteria. The ISME Journal 16, 178–189.

Azúa, I., Goiriena, I., Baña, Z., Iriberri, J., Unanue, M., 2014. Release and Consumption of d-Amino Acids During Growth of Marine Prokaryotes. Microbial Ecology 67, 1–12.

Baumas, C., Bizic, M., 2024. A focus on different types of organic matter particles and their significance in the open ocean carbon cycle. Progress in Oceanography 224, 103233.

Baumas, C., Fuchs, R., Garel, M., Poggiale, J.-C., Memery, L., Le Moigne, F.A.C., Tamburini, C., 2023. Reconstructing the ocean's mesopelagic zone carbon budget: sensitivity and estimation of parameters associated with prokaryotic remineralization. Biogeosciences 20, 4165–4182.

Baumas, C.M.J., Le Moigne, F.A.C., Garel, M., Bhairy, N., Guasco, S., Riou, V., Armougom, F., Grossart, H.-P., Tamburini, C., 2021. Mesopelagic microbial carbon production correlates with diversity across different marine particle fractions. The ISME Journal 15, 1695–1708.

Berthon, J.-F., Zibordi, G., 2004. Bio-optical relationships for the northern Adriatic Sea. International Journal of Remote Sensing 25, 1527–1532.

Bouchachi, N., Obernosterer, I., Marie, B., Crispi, O., Ortega-Retuerta, E., 2023. Phosphorus limitation determines the quality of dissolved organic matter released by marine heterotrophic prokaryotes. Limnology and Oceanography Letters 8, 330–339.

Bouvier, T., Del Giorgio, P.A., Gasol, J.M., 2007. A comparative study of the cytometric characteristics of High and Low nucleic-acid bacterioplankton cells from different aquatic ecosystems. Environmental Microbiology 9, 2050–2066.

Broek, T.A.B., Bour, A.L., Ianiri, H.L., Guilderson, T.P., McCarthy, M.D., 2019. Amino acid enantiomers in old and young dissolved organic matter: Implications for a microbial nitrogen pump. Geochimica et Cosmochimica Acta 247, 207–219.

Bunse, C., Pinhassi, J., 2017. Marine Bacterioplankton Seasonal Succession Dynamics. Trends in Microbiology 25, 494–505.

Buongiorno Nardelli, B., Tronconi, C., Pisano, A., Santoleri, R., 2013. High and Ultra-High resolution processing of satellite Sea Surface Temperature data over Southern European Seas in the framework of MyOcean project. Remote Sensing of Environment 129, 1–16.

Buttigieg, P.L., Fadeev, E., Bienhold, C., Hehemann, L., Offre, P., Boetius, A., 2018. Marine microbes in 4D — using time series observation to assess the dynamics of the ocean microbiome and its links to ocean health. Current Opinion in Microbiology 43, 169–185.

671 Buttigieg, P.L., Ramette, A., 2014. A guide to statistical analysis in microbial ecology: a
672 community-focused, living review of multivariate data analyses. FEMS Microbiology
673 Ecology 90, 543–550.
674 Callahan, B.J., McMurdie, P.J., Rosen, M.J., Han, A.W., Johnson, A.J.A., Holmes, S.P., 2016.
675 DADA2: High-resolution sample inference from Illumina amplicon data. Nature
676 Methods 13, 581–583.
677 Carlson, C.A., Ducklow, H.W., 1995. Dissolved organic carbon in the upper ocean of the
678 central equatorial Pacific Ocean, 1992: Daily and finescale vertical variations. Deep
679 Sea Research Part II: Topical Studies in Oceanography 42, 639–656.
680 Carlson, C.A., Ducklow, H.W., Michaels, A.F., 1994. Annual flux of dissolved organic carbon
681 from the euphotic zone in the northwestern Sargasso Sea. Nature 371, 405–408.
682 Cava, F., Lam, H., De Pedro, M.A., Waldor, M.K., 2011. Emerging knowledge of regulatory
683 roles of d-amino acids in bacteria. Cellular and Molecular Life Sciences 68, 817–831.
684 Charles, F., Lantoine, F., Brugel, S., Chrétiennot-Dinet, M.-J., Quiroga, I., Rivière, B., 2005.
685 Seasonal survey of the phytoplankton biomass, composition and production in a
686 littoral NW Mediterranean site, with special emphasis on the picoplanktonic
687 contribution. Estuarine, Coastal and Shelf Science 65, 199–212.
688 Cherrier, J., Bauer, J., Druffel, E., 1996. Utilization and turnover of labile dissolved organic
689 matter by bacterial heterotrophs in eastern North Pacific surface waters. Marine
690 Ecology Progress Series 139, 267–279.
691 Clementi, E., Pistoia, J., Escudier, R., Delrosso, D., Drudi, M., Grandi, A., Lecci, R., Cretí, S.,
692 Ciliberti, S., Coppini, G., Masina, S., Pinardi, N., 2019. Mediterranean Sea Physical
693 Analysis and Forecast (CMEMS MED-Currents 2016-2019):
694 MEDSEA_ANALYSIS_FORECAST_PHY_006_013.
695 doi:10.25423/CMCC/MEDSEA_ANALYSIS_FORECAST_PHY_006_013_EAS4
696 Copin-Montégut, G., Avril, B., 1993. Vertical distribution and temporal variation of dissolved
697 organic carbon in the North-Western Mediterranean Sea. Deep Sea Research Part I:
698 Oceanographic Research Papers 40, 1963–1972.
699 Dauwe, B., Middelburg, J.J., 1998. Amino acids and hexosamines as indicators of organic
700 matter degradation state inNorth Sea sediments. Limnology and Oceanography 43,
701 782–798.
702 Davis, J., Benner, R., 2007. Quantitative estimates of labile and semi-labile dissolved organic
703 carbon in the western Arctic Ocean: A molecular approach. Limnology and
704 Oceanography 52, 2434–2444.
705 Diaz, F., Naudin, J.-J., Courties, C., Rimmelin, P., Oriol, L., 2008. Biogeochemical and
706 ecological functioning of the low-salinity water lenses in the region of the Rhone
707 River freshwater influence, NW Mediterranean Sea. Continental Shelf Research 28,
708 1511–1526.
709 Escoubeyrou, K., Tremblay, L., 2014. Quantification of free, dissolved combined, particulate,
710 and total amino acid enantiomers using simple sample preparation and more robust
711 chromatographic procedures. Limnology and Oceanography: Methods 12, 421–431.
712 Escudier, R., Clementi, E., Cipollone, A., Pistoia, J., Drudi, M., Grandi, A., Lyubartsev, V., Lecci,
713 R., Aydogdu, A., Delrosso, D., Omar, M., Masina, S., Coppini, G., Pinardi, N., 2021. A
714 High Resolution Reanalysis for the Mediterranean Sea. Frontiers in Earth Science 9,
715 702285.

Evans, C.A., O'Reilly, J.E., Thomas, J.P., 1987. A handbook for the measurement of chlorophyll a and primary production, BIOMASS scientific series. Texas A&M University with support from SCAR, College Station, Texas.
Galand, P.E., Pereira, O., Hochart, C., Auguet, J.C., Debroas, D., 2018. A strong link between marine microbial community composition and function challenges the idea of functional redundancy. The ISME Journal 12, 2470–2478.
Ghiglione, J.-F., Galand, P.E., Pommier, T., Pedrós-Alió, C., Maas, E.W., Bakker, K., Bertilson, S., Kirchman, D.L., Lovejoy, C., Yager, P.L., Murray, A.E., 2012. Pole-to-pole biogeography of surface and deep marine bacterial communities. Proceedings of the National Academy of Sciences 109, 17633–17638.
Giovannoni, S.J., Cameron Thrash, J., Temperton, B., 2014. Implications of streamlining theory for microbial ecology. The ISME Journal 8, 1553–1565.
Gonzalez, M.-L., Blain, S., Obernosterer, I., 2019. Seasonal freshening of NW Mediterranean surface water impacts microbial heterotrophic activity and dissolved organic matter. Estuarine, Coastal and Shelf Science 230, 106448.
González-Dávila, M., Santana-Casiano, J.M., 2023. Long-term trends of pH and inorganic carbon in the Eastern North Atlantic: the ESTOC site. Frontiers in Marine Science 10, 1236214.
Grossart, H.-P., Ploug, H., 2000. Bacterial production and growth efficiencies: Direct measurements on riverine aggregates. Limnology and Oceanography 45, 436–445.
Gutiérrez-Rodríguez, A., Latasa, M., Scharek, R., Massana, R., Vila, G., Gasol, J.M., 2011. Growth and grazing rate dynamics of major phytoplankton groups in an oligotrophic coastal site. Estuarine, Coastal and Shelf Science 95, 77–87.
Hancock, R., 1960. The amino acid composition of the protein and cell wall of Staphylococcus aureus. Biochimica et Biophysica Acta 37, 42–46.
Hansell, D.A., 2013. Recalcitrant Dissolved Organic Carbon Fractions. Annual Review of Marine Science 5, 421–445.
Hayward, A., Pinkerton, M.H., Gutierrez-Rodriguez, A., 2023. PHYTOCLASS: A pigment-based chemotaxonomic method to determine the biomass of phytoplankton classes. Limnology and Oceanography: Methods 21, 220–241.
Hecky, R.E., Mopper, K., Kilham, P., Degens, E.T., 1973. The amino acid and sugar composition of diatom cell-walls. Marine Biology 19, 323–331.
Hsieh, T.C., Ma, K.H., Chao, A., 2016. iNEXT: an R package for rarefaction and extrapolation of species diversity (H ill numbers). Methods in Ecology and Evolution 7, 1451–1456.
Ianiri, H.L., Shen, Y., Broek, T.A.B., McCarthy, M.D., 2022. Bacterial sources and cycling dynamics of amino acids in high and low molecular weight dissolved organic nitrogen in the ocean. Marine Chemistry 241, 104104.
Irazoki, O., Ter Beek, J., Alvarez, L., Mateus, A., Colin, R., Typas, A., Savitski, M.M., Sourjik, V., Berntsson, R.P.-A., Cava, F., 2023. d-amino acids signal a stress-dependent run-away response in Vibrio cholerae. Nature Microbiology 8, 1549–1560.
Jones, V., Meador, T.B., Gogou, A., Migon, C., Penkman, K.E.H., Collins, M.J., Repeta, D.J., 2013. Characterisation and dynamics of dissolved organic matter in the Northwestern Mediterranean Sea. Progress in Oceanography 119, 78–89.
Jørgensen, N., Tranvik, L., Berg, G., 1999. Occurrence and bacterial cycling of dissolved nitrogen in the Gulf of Riga, the Baltic Sea. Marine Ecology Progress Series 191, 1–18.
Kaiser, K., Benner, R., 2008. Major bacterial contribution to the ocean reservoir of detrital organic carbon and nitrogen. Limnology and Oceanography 53, 99–112.

763 Kaiser, K., Benner, R., 2009. Biochemical composition and size distribution of organic matter
764 at the Pacific and Atlantic time-series stations. Marine Chemistry 113, 63–77.
765 Koch, A.L., 2001. Oligotrophs versus copiotrophs. BioEssays 23, 657–661.
766 Laghdass, M., Catala, P., Caparros, J., Oriol, L., Lebaron, P., Obernosterer, I., 2012. High
767 Contribution of SAR11 to Microbial Activity in the North West Mediterranean Sea.
768 Microbial Ecology 63, 324–333.
769 Laghdass, M., West, N.J., Batailler, N., Caparros, J., Catala, P., Lantoine, F., Oriol, L., Lebaron,
770 P., Obernosterer, I., 2010. Impact of lower salinity waters on bacterial heterotrophic
771 production and community structure in the offshore NW Mediterranean Sea.
772 Environmental Microbiology Reports 2, 761–769.
773 Lam, H., Oh, D.-C., Cava, F., Takacs, C.N., Clardy, J., De Pedro, M.A., Waldor, M.K., 2009. D-
774 Amino Acids Govern Stationary Phase Cell Wall Remodeling in Bacteria. Science 325,
775 1552–1555.
776 Lambert, S., Tragin, M., Lozano, J.-C., Ghiglione, J.-F., Vaulot, D., Bouget, F.-Y., Galand, P.E.,
777 2019. Rhythmicity of coastal marine picoeukaryotes, bacteria and archaea despite
778 irregular environmental perturbations. The ISME Journal 13, 388–401.
779 Landa, M., Blain, S., Harmand, J., Monchy, S., Rapaport, A., Obernosterer, I., 2018. Major
780 changes in the composition of a Southern Ocean bacterial community in response to
781 diatom-derived dissolved organic matter. FEMS Microbiology Ecology 94.
782 doi:10.1093/femsec/fiy034
783 Latasa, M., Scharek, R., Vidal, M., Vila-Reixach, G., Gutiérrez-Rodríguez, A., Emelianov, M.,
784 Gasol, J., 2010. Preferences of phytoplankton groups for waters of different trophic
785 status in the northwestern Mediterranean Sea. Marine Ecology Progress Series 407,
786 27–42.
787 Le Moigne, F.A.C., 2019. Pathways of Organic Carbon Downward Transport by the Oceanic
788 Biological Carbon Pump. Frontiers in Marine Science 6, 634.
789 Lemonnier, C., Perennou, M., Eveillard, D., Fernandez-Guerra, A., Leynaert, A., Marié, L.,
790 Morrison, H.G., Memery, L., Paillard, C., Maignien, L., 2020. Linking Spatial and
791 Temporal Dynamic of Bacterioplankton Communities With Ecological Strategies
792 Across a Coastal Frontal Area. Frontiers in Marine Science 7, 376.
793 Liu, C., Cui, Y., Li, X., Yao, M., 2021. *microeco* : an R package for data mining in microbial
794 community ecology. FEMS Microbiology Ecology 97, fiaa255.
795 Liu, S., Baetge, N., Comstock, J., Opalk, K., Parsons, R., Halewood, E., English, C.J.,
796 Giovannoni, S., Bolaños, L.M., Nelson, C.E., Vergin, K., Carlson, C.A., 2020. Stable
797 Isotope Probing Identifies Bacterioplankton Lineages Capable of Utilizing Dissolved
798 Organic Matter Across a Range of Bioavailability. Frontiers in Microbiology 11,
799 580397.
800 Liu, S., Longnecker, K., Kujawinski, E.B., Vergin, K., Bolaños, L.M., Giovannoni, S.J., Parsons,
801 R., Opalk, K., Halewood, E., Hansell, D.A., Johnson, R., Curry, R., Carlson, C.A., 2022.
802 Linkages Among Dissolved Organic Matter Export, Dissolved Metabolites, and
803 Associated Microbial Community Structure Response in the Northwestern Sargasso
804 Sea on a Seasonal Scale. Frontiers in Microbiology 13, 833252.
805 Lomas, M.W., Bates, N.R., Johnson, R.J., Knap, A.H., Steinberg, D.K., Carlson, C.A., 2013. Two
806 decades and counting: 24-years of sustained open ocean biogeochemical
807 measurements in the Sargasso Sea. Deep Sea Research Part II: Topical Studies in
808 Oceanography 93, 16–32.

Love, M.I., Huber, W., Anders, S., 2014. Moderated estimation of fold change and dispersion for RNA-seq data with DESeq2. Genome Biology 15, 550.
Mackey, M., Mackey, D., Higgins, H., Wright, S., 1996. CHEMTAX - a program for estimating class abundances from chemical markers:application to HPLC measurements of phytoplankton. Marine Ecology Progress Series 144, 265–283.
Malmstrom, R.R., Kiene, R.P., Cottrell, M.T., Kirchman, D.L., 2004. Contribution of SAR11 Bacteria to Dissolved Dimethylsulfoniopropionate and Amino Acid Uptake in the North Atlantic Ocean. Applied and Environmental Microbiology 70, 4129–4135.
Many, G., Ulses, C., Estournel, C., Marsaleix, P., 2021. Particulate organic carbon dynamics in the Gulf of Lion shelf (NW Mediterranean) using a coupled hydrodynamic–biogeochemical model. Biogeosciences 18, 5513–5538.
Marty, J.-C., Chiavérini, J., Pizay, M.-D., Avril, B., 2002. Seasonal and interannual dynamics of nutrients and phytoplankton pigments in the western Mediterranean Sea at the DYFAMED time-series station (1991–1999). Deep Sea Research Part II: Topical Studies in Oceanography 49, 1965–1985.
McLaren, M.R., Callahan, B.J., 2021. Silva 138.1 prokaryotic SSU taxonomic training data formatted for DADA2.
McMurdie, P.J., Holmes, S., 2013. phyloseq: An R Package for Reproducible Interactive Analysis and Graphics of Microbiome Census Data. PLoS ONE 8, e61217.
Nunes, S., Latasa, M., Gasol, J., Estrada, M., 2018. Seasonal and interannual variability of phytoplankton community structure in a Mediterranean coastal site. Marine Ecology Progress Series 592, 57–75.
Oksanen, J., Blanchet, F., Friendly, M., Kindt, R., Legendre, P., McGlinn, D., Minchin, P., O'Hara, R., Simpson, G., Solymos, P., Stevens, M., 2022. vegan: Community Ecology Package. R package version 2.5-7. Preprint at 3--1.
Olmedo, E., Taupier-Letage, I., Turiel, A., Alvera-Azcárate, A., 2018. Improving SMOS Sea Surface Salinity in the Western Mediterranean Sea through Multivariate and Multifractal Analysis. Remote Sensing 10, 485.
Olson, R.J., Sosik, H.M., 2007. A submersible imaging-in-flow instrument to analyze nano- and microplankton: Imaging FlowCytobot. Limnology and Oceanography: Methods 5, 195–203.
Ortega-Retuerta, E., Marrasé, C., Muñoz-Fernández, A., Sala, M.M., Simó, R., Gasol, J.M., 2018. Seasonal dynamics of transparent exopolymer particles (TEP) and their drivers in the coastal NW Mediterranean Sea. Science of The Total Environment 631–632, 180–190.
Parada, A.E., Needham, D.M., Fuhrman, J.A., 2016. Every base matters: assessing small subunit rRNA primers for marine microbiomes with mock communities, time series and global field samples: Primers for marine microbiome studies. Environmental Microbiology 18, 1403–1414.
Park, J.T., Strominger, J.L., 1957. Mode of Action of Penicillin: Biochemical Basis for the Mechanism of Action of Penicillin and for Its Selective Toxicity. Science 125, 99–101.
Pawlowicz, R., 2020. M_Map: A mapping package for MATLAB.
Pinhassi, J., Hagström, Å., 2000. Seasonal succession in marine bacterioplankton. Aquatic Microbial Ecology 21, 245–256.
Piontek, J., Handel, N., De Bodt, C., Harlay, J., Chou, L., Engel, A., 2011. The utilization of polysaccharides by heterotrophic bacterioplankton in the Bay of Biscay (North Atlantic Ocean). Journal of Plankton Research 33, 1719–1735.

Poulet, S.A., Martin-Jézéquel, V., 1983. Relationships between dissolved free amino acids, chemical composition and growth of the marine diatom Chaetoceros debile. Marine Biology 77, 93–100.
Puig, P., Palanques, A., Orange, D.L., Lastras, G., Canals, M., 2008. Dense shelf water cascades and sedimentary furrow formation in the Cap de Creus Canyon, northwestern Mediterranean Sea. Continental Shelf Research 28, 2017–2030.
Pujo-Pay, M., Raimbault, P., 1994. improvement of the wet-oxidation procedure for simultaneous determination of particulate organic nitrogen and phosphorus collected on filters. Marine Ecology Progress Series 105, 203–207.
Qian, J., Mopper, K., 1996. Automated High-Performance, High-Temperature Combustion Total Organic Carbon Analyzer. Analytical Chemistry 68, 3090–3097.
Quiroga, I., 2006. Pseudo-Nitzschia Blooms in the Bay of Banyuls-sur-Mer, Northwestern Mediterranean Sea. Diatom Research 21, 91–104.
Ras, J., Claustre, H., Uitz, J., 2008. Spatial variability of phytoplankton pigment distributions in the Subtropical South Pacific Ocean: comparison between in situ and predicted data. Biogeosciences 5, 353–369.
Riedel, T., Dittmar, T., 2014. A Method Detection Limit for the Analysis of Natural Organic Matter via Fourier Transform Ion Cyclotron Resonance Mass Spectrometry. Analytical Chemistry 86, 8376–8382.
Robertson, B.R., Button, D.K., 1989. Characterizing aquatic bacteria according to population, cell size, and apparent DNA content by flow cytometry. Cytometry 10, 70–76.
Romano, S., Dittmar, T., Bondarev, V., Weber, R.J.M., Viant, M.R., Schulz-Vogt, H.N., 2014. Exo-Metabolome of Pseudovibrio sp. FO-BEG1 Analyzed by Ultra-High Resolution Mass Spectrometry and the Effect of Phosphate Limitation. PLoS ONE 9, e96038.
Romera-Castillo, C., Sarmento, H., Álvarez-Salgado, X.A., Gasol, J.M., Marraséa, C., 2010. Production of chromophoric dissolved organic matter by marine phytoplankton. Limnology and Oceanography 55, 446–454.
Roy, S., Llewellyn, C.A., Egeland, E.S., Johnsen, G. (Eds.), 2011. Phytoplankton Pigments: Characterization, Chemotaxonomy and Applications in Oceanography, 1st ed. Cambridge University Press.
Salter, I., Galand, P.E., Fagervold, S.K., Lebaron, P., Obernosterer, I., Oliver, M.J., Suzuki, M.T., Tricoire, C., 2015. Seasonal dynamics of active SAR11 ecotypes in the oligotrophic Northwest Mediterranean Sea. The ISME Journal 9, 347–360.
Sánchez-Pérez, E.D., Pujo-Pay, M., Ortega-Retuerta, E., Conan, P., Peters, F., Marrasé, C., 2020. Mismatched dynamics of dissolved organic carbon and chromophoric dissolved organic matter in the coastal NW Mediterranean Sea. Science of The Total Environment 746, 141190.
Sanchez-Vidal, A., Pasqual, C., Kerhervé, P., Calafat, A., Heussner, S., Palanques, A., Durrieu De Madron, X., Canals, M., Puig, P., 2008. Impact of dense shelf water cascading on the transfer of organic matter to the deep western Mediterranean basin. Geophysical Research Letters 35, 2007GL032825.
Sarmento, H., Romera-Castillo, C., Lindh, M., Pinhassi, J., Sala, M.M., Gasol, J.M., Marrase, C., Taylor, G.T., 2013. Phytoplankton species-specific release of dissolved free amino acids and their selective consumption by bacteria. Limnology and Oceanography 58, 1123–1135.
Schleifer, K.H., Kandler, O., 1972. Peptidoglycan types of bacterial cell walls and their taxonomic implications. Bacteriological Reviews 36, 407–477.

Sebastián, M., Ortega-Retuerta, E., Gómez-Consarnau, L., Zamanillo, M., Álvarez, M., Arístegui, J., Gasol, J.M., 2021. Environmental gradients and physical barriers drive the basin-wide spatial structuring of Mediterranean Sea and adjacent eastern Atlantic Ocean prokaryotic communities. Limnology and Oceanography 66, 4077–4095.

Sherr, E.B., Sherr, B.F., Longnecker, K., 2006. Distribution of bacterial abundance and cell-specific nucleic acid content in the Northeast Pacific Ocean. Deep Sea Research Part I: Oceanographic Research Papers 53, 713–725.

Siegel, D.A., Buesseler, K.O., Behrenfeld, M.J., Benitez-Nelson, C.R., Boss, E., Brzezinski, M.A., Burd, A., Carlson, C.A., D'Asaro, E.A., Doney, S.C., Perry, M.J., Stanley, R.H.R., Steinberg, D.K., 2016. Prediction of the Export and Fate of Global Ocean Net Primary Production: The EXPORTS Science Plan. Frontiers in Marine Science 3. doi:10.3389/fmars.2016.00022

Smith, D.C., Simon, M., Alldredge, A.L., Azam, F., 1992. Intense hydrolytic enzyme activity on marine aggregates and implications for rapid particle dissolution. Nature 359, 139–142.

Sosik, H.M., Olson, R.J., 2007. Automated taxonomic classification of phytoplankton sampled with imaging-in-flow cytometry. Limnology and Oceanography: Methods 5, 204–216.

Sugimura, Y., Suzuki, Y., 1988. A high-temperature catalytic oxidation method for the determination of non-volatile dissolved organic carbon in seawater by direct injection of a liquid sample. Marine Chemistry 24, 105–131.

Teeling, H., Fuchs, B.M., Bennke, C.M., Krüger, K., Chafee, M., Kappelmann, L., Reintjes, G., Waldmann, J., Quast, C., Glöckner, F.O., Lucas, J., Wichels, A., Gerdts, G., Wiltshire, K.H., Amann, R.I., 2016. Recurring patterns in bacterioplankton dynamics during coastal spring algae blooms. eLife 5, e11888.

Thingstad, T.F., Hagström, Å., Rassoulzadegan, F., 1997. Accumulation of degradable DOC in surface waters: Is it caused by a malfunctioning microbial loop? Limnology and Oceanography 42, 398–404.

Trano, A.C., Piredda, R., Balestra, C., Bastianini, M., Gasol, J.M., Casotti, R., 2022. Diversity of Free-Living and Particle-Attached Prokaryotes in a River-Influenced Coastal Area of the Northern Adriatic Sea. Frontiers in Marine Science 9, 912528.

Vila-Reixach, G., Gasol, J., Cardelús, C., Vidal, M., 2012. Seasonal dynamics and net production of dissolved organic carbon in an oligotrophic coastal environment. Marine Ecology Progress Series 456, 7–19.

Volpe, G., Buongiorno Nardelli, B., Colella, S., Pisano, A., Santoleri, R., 2018. An Operational Interpolated Ocean Colour Product in the Mediterranean Sea, in: Chassignet, E.P., Pascual, A., Tintoré, J., Verron, J. (Eds.), New Frontiers in Operational Oceanography. GODAE OceanView. doi:10.17125/gov2018.ch09

Volpe, G., Colella, S., Brando, V.E., Forneris, V., La Padula, F., Di Cicco, A., Sammartino, M., Bracaglia, M., Artuso, F., Santoleri, R., 2019. Mediterranean ocean colour Level 3 operational multi-sensor processing. Ocean Science 15, 127–146.

von Jackowski, A., Becker, K.W., Wietz, M., Bienhold, C., Zäncker, B., Nöthig, E., Engel, A., 2022. Variations of microbial communities and substrate regimes in the eastern Fram Strait between summer and fall. Environmental Microbiology 24, 4124–4136.

von Jackowski, A., Bouchachi, N., Labatut, P., Marie, Barbara, B., Crispi, O., Escoubeyrou, K., Paulin, C.-H., Dimier, C., Ras, Ortega-Retuerta, E., 2024. Phytoplankton and DOM at MOLA 2019-2021. doi:10.1594/PANGAEA.967436

von Jackowski, A., Grosse, J., Nöthig, E.-M., Engel, A., 2020. Dynamics of organic matter and bacterial activity in the Fram Strait during summer and autumn. Philosophical Transactions of the Royal Society A: Mathematical, Physical and Engineering Sciences 378, 20190366.

Wagner, S., Schubotz, F., Kaiser, K., Hallmann, C., Waska, H., Rossel, P.E., Hansman, R., Elvert, M., Middelburg, J.J., Engel, A., Blattmann, T.M., Catalá, T.S., Lennartz, S.T., Gomez-Saez, G.V., Pantoja-Gutiérrez, S., Bao, R., Galy, V., 2020. Soothsaying DOM: A Current Perspective on the Future of Oceanic Dissolved Organic Carbon. Frontiers in Marine Science 7, 341.

Wickham, H., 2016. ggplot2: Elegant Graphics for Data Analysis. Springer-Verlag New York.

Wilson, B., Müller, O., Nordmann, E.-L., Seuthe, L., Bratbak, G., Øvreås, L., 2017. Changes in Marine Prokaryote Composition with Season and Depth Over an Arctic Polar Year. Frontiers in Marine Science 4. doi:10.3389/fmars.2017.00095

Winkler, L.W., 1888. Die Bestimmung des im Wasser gelösten Sauerstoffes. Berichte der deutschen chemischen Gesellschaft 21, 2843–2854.

Wirtz, K., Smith, S.L., 2020. Vertical migration by bulk phytoplankton sustains biodiversity and nutrient input to the surface ocean. Scientific Reports 10, 1142.

Yamashita, Y., Tanoue, E., 2003. Chemical characterization of protein-like fluorophores in DOM in relation to aromatic amino acids. Marine Chemistry 82, 255–271.

Yu, Y., Yang, J., Zheng, L.-Y., Sheng, Q., Li, C.-Y., Wang, M., Zhang, X.-Y., McMinn, A., Zhang, Y.-Z., Song, X.-Y., Chen, X.-L., 2020. Diversity of D-Amino Acid Utilizing Bacteria From Kongsfjorden, Arctic and the Metabolic Pathways for Seven D-Amino Acids. Frontiers in Microbiology 10, 2983.

Zhang, G., Sun, H.J., 2014. Racemization in Reverse: Evidence that D-Amino Acid Toxicity on Earth Is Controlled by Bacteria with Racemases. PLoS ONE 9, e92101.

Zhang, Z., Zheng, Q., Jiao, N., 2016. Microbial D-amino acids and marine carbon storage. Science China Earth Sciences 59, 17–24.

Zhao, Z., Gonsior, M., Luek, J., Timko, S., Ianiri, H., Hertkorn, N., Schmitt-Kopplin, P., Fang, X., Zeng, Q., Jiao, N., Chen, F., 2017. Picocyanobacteria and deep-ocean fluorescent dissolved organic matter share similar optical properties. Nature Communications 8, 15284.

Figures

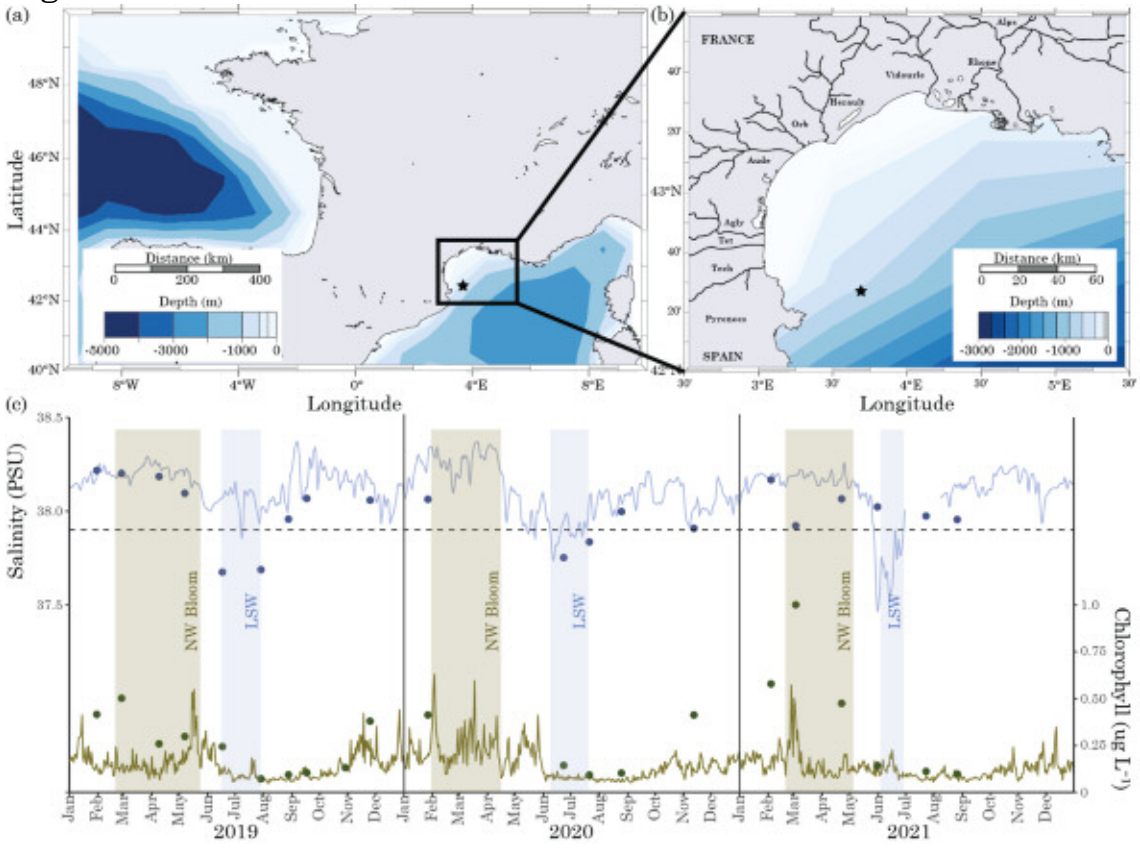

Figure 1. Bathymetry and temporal conditions at Microbial Observatory Laboratory Arago (MOLA) in the northwestern Mediterranean Sea between 2019 and 2021. The MOLA time series station (star) is located off (a) northern Catalonia in the (b) drainage basin of the Agly, Aude, Hérault, Orb, Rhône, Tech, Têt, and Vidourle into the Gulf of Lyon. The (c) satellite-derived (line) and subsurface (5 m, circles) of salinity (blue) and chlorophyll-a (green) at MOLA. Remote sensing allowed for a differentiation between coastal and offshore northwestern blooms. Low salinity water (LSW) events are below 37.9 PSU (dashed line) for more than three consecutive days.

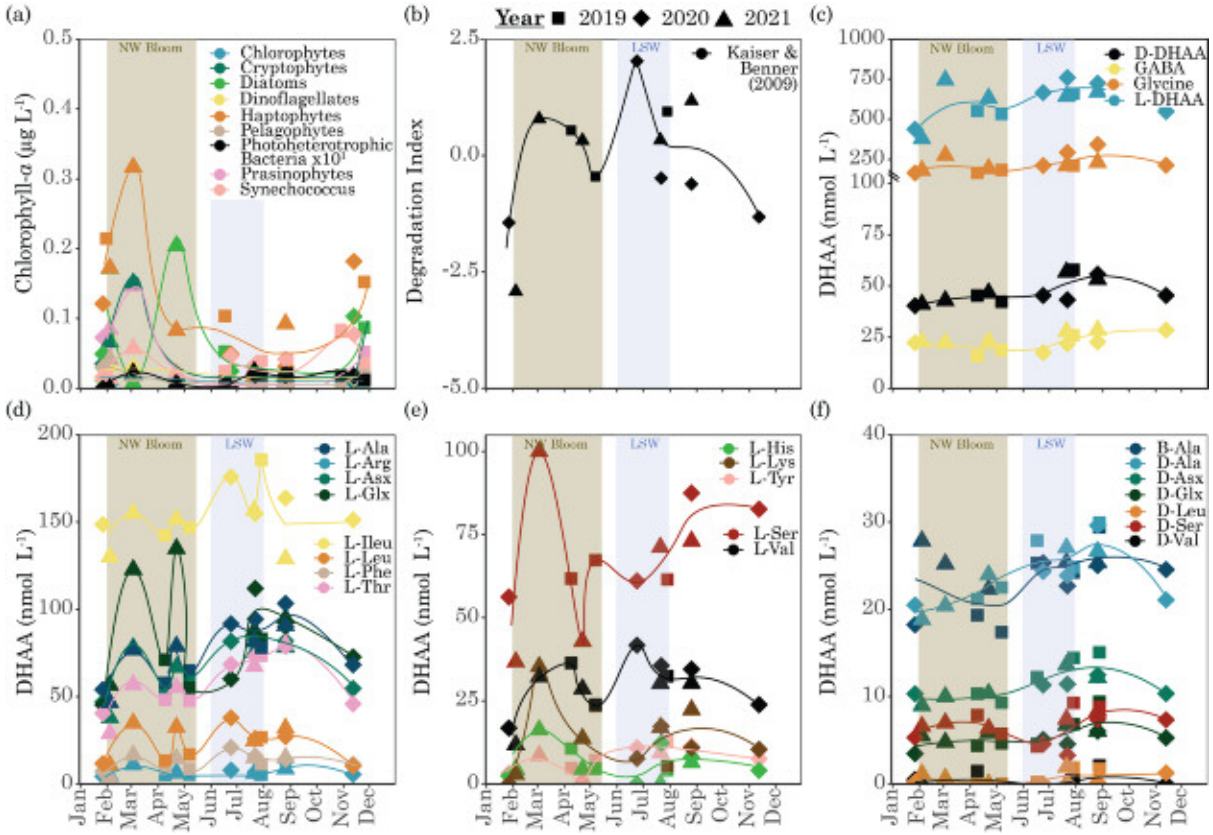

Figure 2. Seasonal dynamics of phytoplankton biomass and dissolved hydrolyzable amino acids (DHAA) at 5 meters of the Microbial Observatory Laboratory Arago. The (a) phytoplankton biomass estimated from pigment biomarkers and bacteriochlorophyll-a for photoheterotrophic bacteria, (b) DHAA degradation index, (c) total concentrations of L- and D-DHAA and non-isomers gamma-aminobutyric acid (GABA) and glycine, (d) L-DHAA that peak twice during the NWMED bloom, (e) L-DHAA that only peak once during the NWMED bloom, (f) B- and D-DHAA. The shape corresponds to the year and abbreviations refer to: Ala, Alanine; Asx, Aspartic acid and Asparagine; Arg, Arginine; Glx, Glutamic acid and Glutamine; His, Histidine; Ileu, Isoleucine; Leu, Leucine; Lys, Lysine; Phe, Phenylalanine; Ser, Serine; Thr, Threonine; Tyr, Tyrosine; Val, Valine.

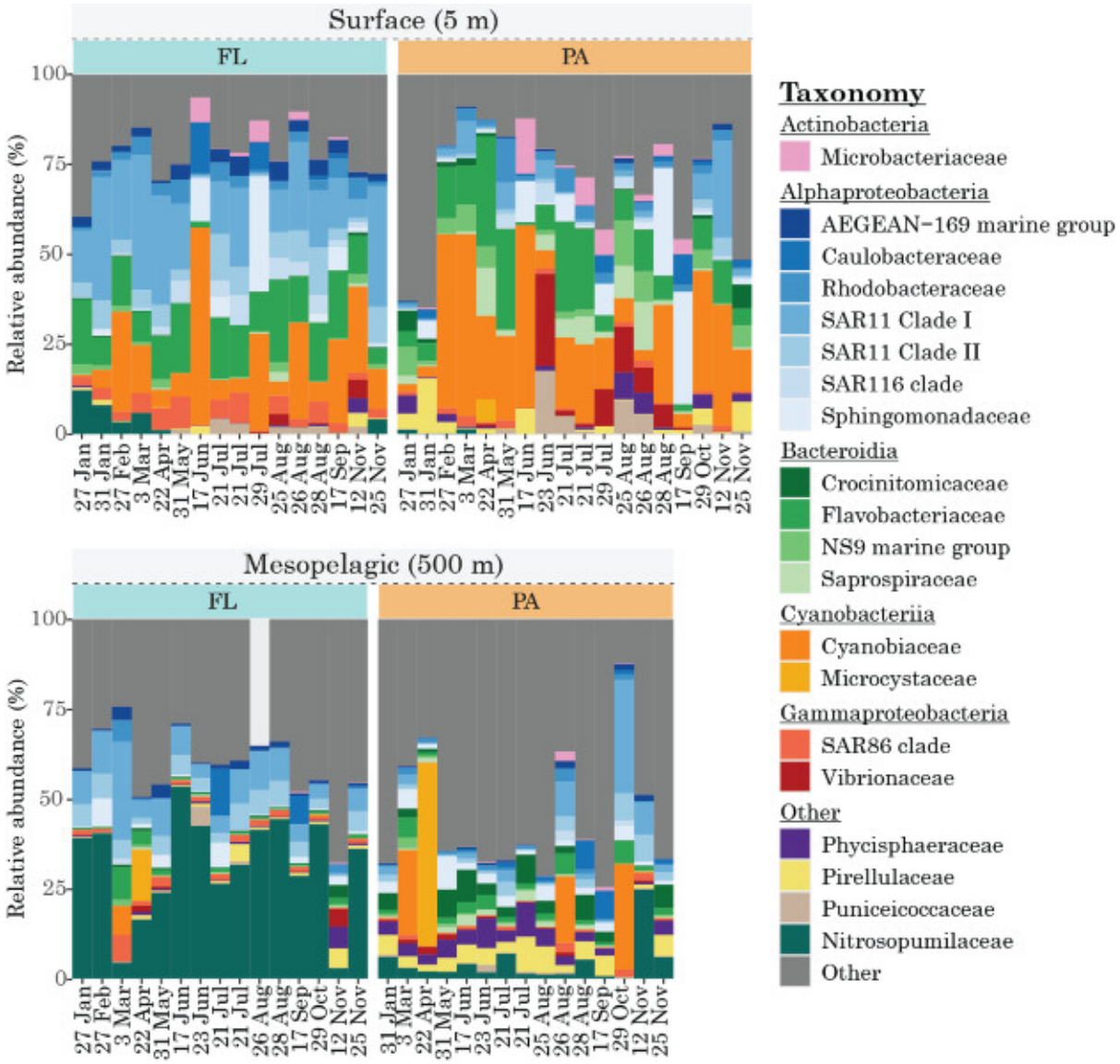

Figure 3. Seasonal dynamics of the top 20 bacterioplankton families at the Microbial Observatory Laboratory Arago. Dominant orders in the free-living (FL) and particle-attached (PA) community at 5 m and 500 m depth.

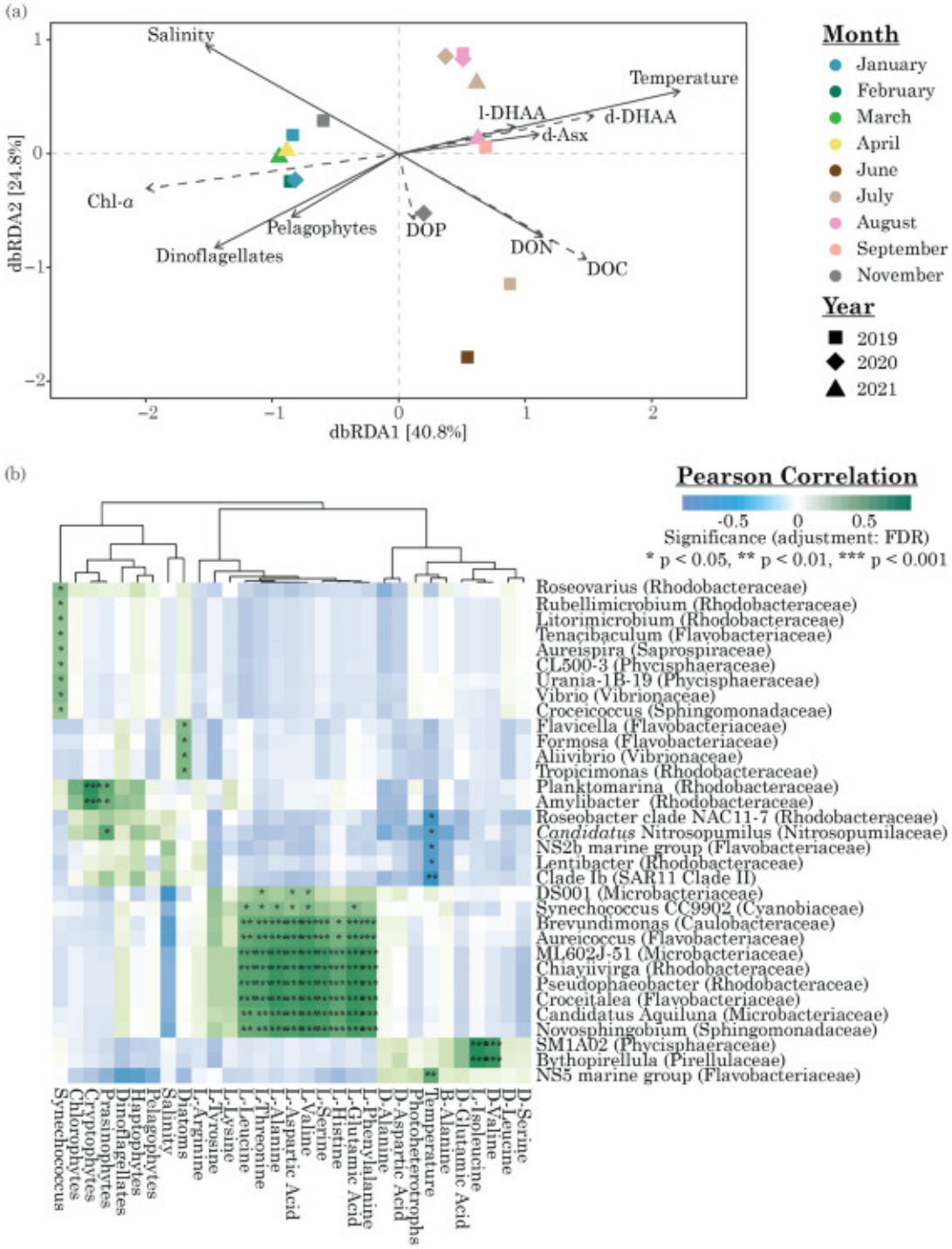

Figure 4. Links between DOM and the free-living (FL) bacterioplankton community at 5 meters of the Microbial Observatory Laboratory Arago. The redundancy analysis shows the significant environmental parameters and ordination of the samples. A (b) pearson correlation between environmental parameters and the bacterioplankton community at genus level within the top 20 families and false discovery rate (FDR) adjusted p-values (* p<0.05, ** p<0.01, *** p<0.001). Abbreviations refer to: Asx, Aspartic acid and Asparagine; Chl-a, Chlorophyll-a; dissolved hydrolyzable amino acid, DHAA; dissolved organic carbon, DOC; dissolved organic nitrogen, DON; dissolved organic phosphorus, DOP.